Journal of Magnetic Resonance 304 (2019) 78–86

Contents lists available at ScienceDirect

Journal of Magnetic Resonance

journal homepage: www.elsevier.com/locate/jmr

Resolution enhancement and proton proximity probed by 3D TQ/DQ/SQ proton NMR spectroscopy under ultrafast magic-angle-spinning beyond 70 kHz

Rongchun Zhang [a,*,1], Nghia Tuan Duong [b,1], Yusuke Nishiyama [b,c,*]

[a] South China Advanced Institute for Soft Matter Science and Technology (AISMST), School of Molecular Science and Engineering, South China University of Technology, Guangzhou 510640, PR China
[b] NMR Science and Development Division, RIKEN SPring-8 Center, and Nano-Crystallography Unit, RIKEN-JEOL Collaboration Center, Yokohama, Kanagawa 230-0045, Japan
[c] JEOL RESONANCE Inc., Musashino, Akishima, Tokyo 196-8558, Japan

ARTICLE INFO

Article history:
Received 10 April 2019
Revised 15 May 2019
Accepted 18 May 2019
Available online 21 May 2019

Keywords:
Solid-state NMR
Triple-quantum
Double-quantum
Proton detection
Ultrafast MAS

ABSTRACT

Proton nuclear magnetic resonance (NMR) in solid state has gained significant attention in recent years due to the remarkable resolution and sensitivity enhancement afforded by ultrafast magic-angle-spinning (MAS). In spite of the substantial suppression of ^{1}H-^{1}H dipolar couplings, the proton spectral resolution is still poor compared to that of ^{13}C or ^{15}N NMR, rendering it challenging for the structural and conformational analysis of complex chemicals or biological solids. Herein, by utilizing the benefits of double-quantum (DQ) and triple-quantum (TQ) coherences, we propose a 3D single-channel pulse sequence that correlates proton triple-quantum/double-quantum/single-quantum (TQ/DQ/SQ) chemical shifts. In addition to the two-spin proximity information, this 3D TQ/DQ/SQ pulse sequence enables more reliable extraction of three-spin proximity information compared to the regular 2D TQ/SQ correlation experiment, which could aid in revealing the proton network in solids. Furthermore, the TQ/DQ slice taken at a specific SQ chemical shift only reveals the local correlations to the corresponding SQ chemical shift, and thus it enables accurate assignments of the proton peaks along the TQ and DQ dimensions and simplifies the interpretation of proton spectra especially for dense proton networks. The high performance of this 3D pulse sequence is well demonstrated on small compounds, *L*-alanine and a tripeptide, N-formyl-*L*-methionyl-*L*-leucyl-*L*-phenylalanine (MLF). We expect that this new methodology can inspire the development of multidimensional solid-state NMR pulse sequences using the merits of TQ and DQ coherences and enable high-throughput investigations of complex solids using abundant protons.

1. Introduction

Solid-state NMR spectroscopy has well demonstrated itself as a powerful tool for high-throughput investigation on non-soluble and non-crystalline chemicals and biological solids [1–9]. Despite the significant advances in the last few decades on methodologies and hardware, spectral resolution and sensitivity is still a bottleneck for the application of solid-state NMR spectroscopy in various challenging molecular systems, such as bone [10,11], membrane proteins [12,13] and amyloids [14–16], in particular for proton NMR. Although proton is an abundant nucleus in nature (>99.9%), it has rarely been utilized in solid-state NMR due to the severe line broadening induced by the strong ^{1}H-^{1}H dipolar couplings, leading to a significant loss of site-specific structural information [17,18]. Therefore, tremendous efforts have been devoted into suppressing the dipolar couplings by manipulating either the spin- or spatial interactions of protons. One example is to use a combined rotation and multiple pulse decoupling schemes (i.e. CRAMPS) [19]. However, the setup of CRAMPS experiment is not trivial, especially the scaling of chemical shifts, and the signal-to-noise ratios are often compromised due to the large filter bandwidth of receivers and potentially low quality factor of probes. Another more straightforward approach, with significantly simplified setup, is to use magic-angle-spinning (MAS), whose frequency can be up to 140 kHz using tiny rotors with a diameter of 0.51 mm [20].

* Corresponding authors at: South China Advanced Institute for Soft Matter Science and Technology (AISMST), School of Molecular Science and Engineering, South China University of Technology, Guangzhou, 510640, P. R. China (R. Zhang), NMR Science and Development Division, RIKEN SPring-8 Center, and Nano-Crystallography Unit, RIKEN-JEOL Collaboration Center, Yokohama, Kanagawa 230-0045, Japan (Y. Nishiyama).
E-mail addresses: zhangcr@scut.edu.cn (R. Zhang), yunishiy@jeol.co.jp (Y. Nishiyama).
[1] These authors have contributed equally to this work.

https://doi.org/10.1016/j.jmr.2019.05.006
1090-7807/

Under ultrafast MAS conditions ($\upsilon_R \geq 60$ kHz), the proton homonuclear dipolar couplings can be substantially suppressed, because the dominating higher-order terms in the multi-spin proton-proton dipolar Hamiltonian are inversely proportional to the spinning frequency [21–23]. As a result, tremendous enhancement of proton spectral resolution can be achieved under ultrafast MAS, shedding substantial light on using proton detection in multidimensional solid-state NMR spectroscopy [24–30]. Even though anisotropic bulk magnetic susceptibility (ABMS) [31,32], which is only partially averaged out by MAS, imposes limits on the ^{1}H linewidth at very fast MAS, because of its high gyromagnetic ratio and abundance, proton detection in solid state has gained huge popularity in recent years [33–48]. Proton-detected heteronuclear correlation NMR experiment has become a routine approach for revealing the heteronuclear proximity in NMR crystallography [38,49–55]. In combination with appropriate deuteration schemes and external high magnetic field, solution-like proton spectra can be easily obtained even in proteins; thus multidimensional proton-detected solid-state NMR spectroscopy has been widely used for the conformational analyses and site-specific dynamic studies [24,40,56–58]. Through proton driven spin diffusion and proton detection, even homonuclear ^{15}N/^{15}N chemical shift correlation can be achieved within a total experiment time of less than 5 h in a manner of 3D ^{15}N/^{15}N/^{1}H chemical shift correlation experiment [59]. Moreover, site-specific measurement of proton chemical shift anisotropy (CSA) tensor has also become possible [60–63], leading to a fruitful structural investigations on crystalline polymorphs and pharmaceuticals, in particular when the proton CSAs are correlated with high-resolution low-γ nuclei chemical shift dimensions [64–66].

Among all the proton-based NMR approaches, single-channel multidimensional proton NMR spectroscopy is the most attractive, since it can take full advantages of high natural abundance and sensitivity of protons [17,67,68]. For example, ^{1}H/^{1}H single-quantum/single-quantum (SQ/SQ) chemical shift correlation experiment directly provides the proximity information of two protons, but it also gives strong diagonal peaks, which can blur weak correlation cross-peaks near the diagonal line [69,70]. Two-spin proximity is more frequently probed in a manner of double-quantum/single-quantum (DQ/SQ) chemical shift correlations, since the absences of isolated diagonal peaks greatly simplify the spectral analysis; all the peaks appear in DQ/SQ experiments come from two-spin correlations. In addition, the DQ dimension has a doubled spectral width compared to the SQ dimension [71]. Using the enhanced spectral resolution offered by the DQ coherence, the proton CSA of overlapped chemical shifts can be even determined by implementing ^{1}H DQ/CSA/SQ correlation experiment [63]. In order to fully exploring the benefits of DQ coherence, previously we also reported studies on ^{1}H SQ/DQ/SQ [72] and DQ/DQ/SQ [73] chemical shift correlation experiments demonstrating the additional possibilities and applications. The ^{1}H SQ/DQ/SQ experiment can reveal information on the proximity between a spin and a certain other dipolar-coupled pair of spins [72], while ^{1}H DQ/DQ/SQ experiment enables the extraction of both three-spin and four-spin proximity information, which is greatly beneficial for revealing the 3D proton network in the solid state [73]. It is worth noting that the three-spin proximity can be directly revealed in the triple-quantum (TQ) coherence [71,74–76]. However, TQ/SQ experiment has rarely been explored in dense proton systems due to the difficulty and ambiguity in assigning the TQ peaks. Herein, to fully exploiting the advantages of TQ and DQ coherences, we further propose a proton TQ/DQ/SQ chemical shift correlation experiment. In addition to two-spin and three-spin proximity information as revealed in regular 2D DQ/SQ and TQ/SQ experiments, the additional TQ/DQ slices provide site-specific information related to the local proton network indicated by the specific SQ chemical shifts. Therefore, the TQ and DQ peaks along the TQ and DQ dimensions respectively, can be accurately assigned. Thus, this 3D TQ/DQ/SQ experiment can provide two-spin and more precise three-spin proximity information in a higher resolution manner compared to the regular 2D experiments. In this study, we firstly demonstrate the feasibility of the proposed method on a small molecule, *L*-alanine, and then further use it to explore the proton network in a tripeptide, N-formyl-*L*-methionyl-*L*-leucyl-*L*-phenylalanine (MLF).

2. Experimental

2.1. Samples

Uniformly ^{13}C, ^{15}N-L-alanine was purchased from Isotec. (Champaign, IL). Naturally abundant tripeptide (N-formyl-*L*-methionyl-*L*-leucyl-*L*-phenylalanine, referred as MLF) was purchased from Sigma-Aldrich. Both samples were used as received without any further purification.

2.2. Solid-state NMR spectroscopy

NMR measurements on alanine and MLF were carried out at 600 MHz and 900 MHz solid-state NMR spectrometer (JEOL RESONANCE Inc., JNM-ECZ600R and ECZ900R), equipped with a 1.0 mm double-resonance and triple-resonance ultrafast MAS probe (JEOL RESONANCE Inc.) operating at ^{1}H Larmor frequencies of 599.67 MHz and 899.44 MHz, respectively. The nominal ^{1}H 90° pulse length was 1.1 μs on both 600 and 900 MHz solid-state NMR spectrometer. Recycle delay was set as 1.5 s for alanine and 2.5 s for MLF sample. The MAS rate was set as 70 and 72 kHz for the measurement on alanine and MLF sample, respectively. The 3D ^{1}H TQ/DQ/SQ pulse sequence and its coherence pathway are shown in Fig. 1. For exciting the DQ coherence, the dipolar recoupling pulse sequence, BABA-xy16 [77], was adapted, since it is easy to setup and robust to the offset and RF inhomogeneity. For exciting the TQ coherences, we applied a 90° pulse before the implementation of BABA-xy16 pulse sequence, so the coherence order would change from 0 to ±3. The TQ chemical shift was evolved during the t_1 period (i.e. t_1 evolution). Following the t_1 evolution, a rectangular conversion pulse was applied to induce DQ coherences since the coherence order would change from +3 → −2 and −3 → +2. As the two BABA sequences and t_1 and t_2 evolution times should be rotor-synchronized for accurate positioning of the center bands as well as increasing their sensitivities due to the folding of spinning sidebands, a delay was inserted right before the DQ chemical shift evolution (i.e. t_2 evolution) so that the total length of the conversion pulse and the delay is a rotor period. Thus, it requires a phase correction in the t_2 dimension for obtaining in-phase 2D/3D spectra. Finally, the DQ coherence was reconverted to the magnetization along the z direction (I_{nz}) by the second BABA-xy16 sequence, and then to SQ by the 90° read pulse after the z-filter, which was used to suppress the residual transverse magnetization after the DQ reconversion period. The z-filter time (t_{zf}) was usually set as 1 ms. A 6- and 10-step phase cycles were adapted to obtain the pure TQ and DQ coherence evolution in the t_1 and t_2 period, respectively, resulting in a total of minimum 60 steps phase cycling. If t_{zf} of 1 ms is not sufficient for complete suppression of the residual transverse magnetization, the 3-step phase cycle of the read pulse (φ_3) can be further used. While 60-step phase cycle is adopted in the current study, the number of scans can be reduced to 24 steps (6 steps for TQ excitation, 4 steps for DQ BABA reconversion, and 1 ms z-filter as shown in Fig. S1). This can further reduce the experimental time, given the sensitivity is sufficient. The length of BABA-xy16 recoupling time is eights rotor

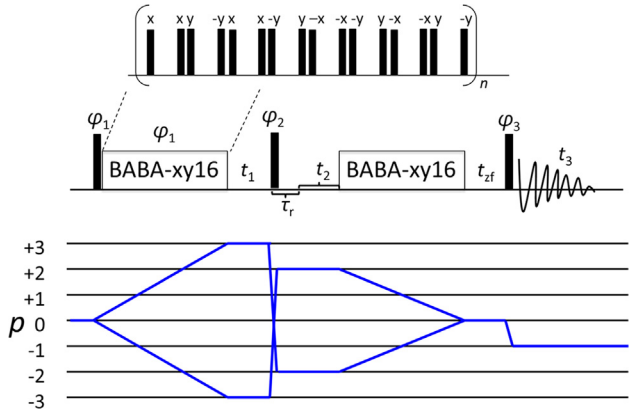

Fig. 1. Single-channel 3D ^{1}H TQ/DQ/SQ pulse sequence. A single 90° pulse was employed before the first BABA-xy16 block to together excite the TQ coherences, followed by the evolution of the TQ chemical shifts (i.e. t_1 evolution). A rectangular conversion pulse was applied after the t_1 evolution to induce DQ coherences, where a short delay ($\tau_r - t_p$, τ_r is the rotor period, and t_p is the pulse length of the conversion pulse) was inserted before the t_2 evolution to ensure the rotor-synchronization condition. The phase cycling scheme used in this 3D pulse sequence is as follows: φ_1 = {0, 60°, 120°, 180°, 240°, 300°},φ_2 = {6(0°), 6(36°), 6(72°), 6(108°), 6(144°), 6(180°), 6(216°), 6(252°), 6(288°), 6(324°)},φ_3 = {60(0°), 60(120°), 60(240°)},φ_{rec} = {5(3(0°, 180°), 3(180°, 0°)), 5(3(120°, 300°), 3(300°, 120°)), 5(3(240°, 60°), 3(60°, 240°))}. t_{zf} was set as 1 ms.

periods, corresponding to 114.3 μs and 111.1 μs for the measurement on alanine (MAS of 70 kHz) and MLF (MAS of 72 kHz), respectively. States-TPPI method was used for the signal acquisition of both t_1 and t_2 periods [78].

3. Results and discussion

The 2D NMR spectrum generally gives a higher resolution compared to the regular 1D spectrum due to the incorporation of the second dimension. Better separation of peaks can be achieved when DQ coherence evolution is incorporated into the second dimension due to the doubled spectral width, and thus 2D DQ/SQ experiment has been widely used for probing proton proximity and resonance assignments. Note that the inhomogeneous linewidths of the peaks along the DQ dimension are doubled compared to those in the SQ dimension, and thus will partially offset the benefits of wider spectral width in the DQ dimension [79]. Larger separations of peaks can be further achieved on the TQ dimension compared to DQ; however, the number of peaks in the TQ dimension also significantly increase. This generally leads to ambiguous assignments of correlation peaks especially when there are dense protons, hampering the practical applications of TQ/SQ experiments. In this study, by further expanding the 2D experiment into a 3D experiment and correlating the TQ/DQ chemical shifts, the proposed 3D TQ/DQ/SQ experiment here can provide much higher spectral resolution and can be used to probe multi-spin proximity and enable more accurate resonance assignments. The feasibility and principle of this 3D sequence is firstly discussed using a simple small molecule, *L*-alanine, and then its superior performance is further demonstrated on a tripeptide (MLF) with a higher proton density.

3.1. Multiple-Quantum (MQ) transition efficiency

Since there are multiple MQ transition processes involved in the proposed 3D sequence, it is better to know the overall MQ transition efficiency for better understanding the performance of this new 3D experiment. Thus, we also implemented the regular 2D TQ/SQ and DQ/SQ experiments (Fig. S2) and the obtained 1D spectra (i.e. $t_1 = 0$) were used to compare the MQ transition efficiency with that of 3D experiment (i.e. $t_1 = t_2 = 0$). The results on alanine are shown in Fig. 2, and the intensity comparison is also summarized in Table 1. Notably, starting from the same initial equilibrium state for all experiments, the $I_{nz} \rightarrow TQ \rightarrow DQ \rightarrow SQ$ transition efficiency in the 3D experiment ($\varepsilon_{Inz\rightarrow TQ\rightarrow DQ\rightarrow SQ}$) is roughly equal to the product of $I_{nz} \rightarrow DQ \rightarrow SQ$ transition efficiency ($\varepsilon_{Inz\rightarrow DQ\rightarrow SQ}$) and $I_{nz} \rightarrow TQ \rightarrow SQ$ transition efficiency ($\varepsilon_{Inz\rightarrow TQ\rightarrow SQ}$) in the 2D DQ/SQ and TQ/SQ correlation experiments, respectively, although there is finite time chemical shift evolution ($\tau_r - t_p$) after the TQ → DQ transition in the 3D experiment. Therefore, it well demonstrates that there is basically no additional signal loss in the 3D TQ/DQ/SQ correlation experiment except the MQ transitions. In average, the resulted $I_{nz} \rightarrow TQ \rightarrow DQ \rightarrow SQ$ transition efficiency in the 3D experiment is around 2% with respect to the spin echo spectrum. Due to the high gyromagnetic ratio of ^{1}H nuclei as well as its high natural abundance (>99.9%), even a 2% signal intensity is sufficient for the implementation of 3D TQ/DQ/SQ experiment as will be shown below. Note that in the current 3D sequence, the BABA-xy16 sequence requires a minimum DQ recoupling time of $8\tau_R$, where τ_R is the rotor period. However, for the rigid crystalline compounds, such as *L*-alanine here, a long recoupling time may lead to reduced DQ recoupling efficiency in comparison to the maximum theoretical value of ~73%. Therefore, other DQ recoupling sequences, such as broadband BABA [80] or SPIP [81], can be adopted since shorter DQ recoupling time can be used for improving the DQ efficiency.

3.2. 3D TQ/DQ/SQ spectrum of L-alanine at 70 kHz MAS and 600 MHz magnetic field

After initial optimization of the parameters in the pulse sequences, the 3D experiment was performed on a powder sample of L-alanine at 70 kHz MAS. The optimized results of different

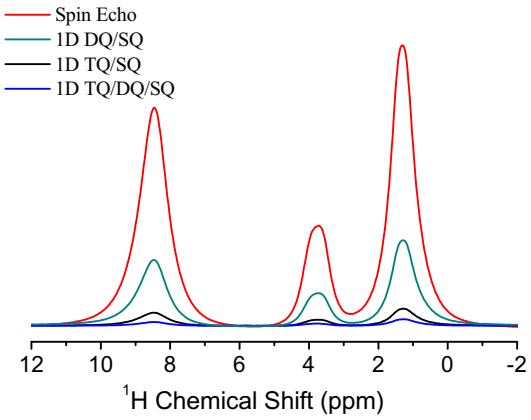

Fig. 2. Comparison of 1D proton spectra of alanine at 600 MHz and 70 kHz obtained by 1D spin echo, DQ/SQ ($I_{nz} \rightarrow DQ \rightarrow SQ$), TQ/SQ ($I_{nz} \rightarrow TQ \rightarrow SQ$) and TQ/DQ/SQ ($I_{nz} \rightarrow TQ \rightarrow DQ \rightarrow SQ$) experiments. The inter-pulse delay between 90° and 180° pulse in the spin echo experiment was set as one rotor period.

Table 1
Comparison of MQ transition efficiencies. All the transition efficiency values are obtained by intensity normalization with respect to that of 1D spin echo spectrum.

Transition efficiency	NH_3^+ (8.4 ppm)	—CH (3.7 ppm)	—CH_3 (1.3 ppm)
Spin Echo	100%	100%	100%
$\varepsilon_{Inz\rightarrow DQ\rightarrow SQ}$ (1D DQ/SQ)	31.0%	32.2%	30.4%
$\varepsilon_{Inz\rightarrow TQ\rightarrow SQ}$ (1D TQ/SQ)	6.4%	7.3%	6.0%
$\varepsilon_{Inz\rightarrow TQ\rightarrow DQ\rightarrow SQ}$ (1D TQ/DQ/SQ)	1.7%	2.1%	2.3%

parameters, including 90° pulse lengths in the first and second BABA-xy16 recoupling periods, and the duration of the TQ → DQ conversion pulse, are included in the Supporting Information (Figs. S3–S5). The nominal ^{1}H 90° pulse length is around 1.1 μs as optimized using single-pulse experiment. However, such value does not provide the optimum BABA-xy16 recoupling efficiency as shown in Figs. S3 and S4. Notably, the 90° pulse length for the optimal BABA recoupling efficiency is both around 0.65 μs, which is quite different from the nominal duration of the 90° pulse. In fact, such phenomenon was already previously reported [26], but still not well understood so far. It is speculated that multi-spin dipolar couplings may play a significant role in inducing the DQ ↔ I_{nz} transition. An in-depth theoretical understanding is required; however, this is out of the scope of the current study. The optimum length of the TQ → DQ conversion pulse is 1.7 μs as shown in Fig. S5. Fig. 3 shows the comparison of DQ/SQ and TQ/SQ spectra obtained from regular 2D experiments (Fig. 3a and b) and the corresponding projected 2D spectra from 3D TQ/DQ/SQ spectrum (Fig. 3c and d). An important difference between the regular 2D DQ/SQ and projected 2D DQ/SQ is the characteristics of DQ terms. For the former, the DQ Hamiltonian between two spins is $I_1^+I_2^+ + I_1^-I_2^-$, where I is the spin angular momentum vector operator; hence, the DQ correlation only involves two spins as observed in Fig. 3a. For the latter, as the DQ is created from the TQ coherences and if the three spins are spatially close, the DQ Hamiltonian actually involves three spins, i.e. $(I_1^+I_2^+ + I_1^-I_2^-)I_{3z}$. Consequently, for *L*-alanine, in the projected 2D DQ/SQ, the (*A*,*B*) DQ correlation peak will also correlate with the SQ chemical shift of spin *C*. Such phenomenon is evident for the highlighted peaks (red circles) in Fig. 3c. For example, for the DQ peak *AA* in Fig. 3c, its correlations with spin *B* and *C* are still observed. However, this should not be understood as the four-spin proximity but the two pairs of three-spin proximity, including (*AA*)-*B* and (*AA*)-*C*. It is worth noting that there is a clear autocorrelation peak of proton *B* (i.e. methine protons) in the regular 2D DQ/SQ spectrum (Fig. 3a); however, such correlation is negligible in the projected 2D DQ/SQ spectrum (Fig. 3c). This difference in intensity is because the DQ coherences of the projected spectrum are converted from the TQ coherences in the 3D experiments, suffering from an additional signal loss in I_{nz} → TQ → DQ transitions. If the intensity of TQ coherences is weak and/or the TQ → DQ conversion is not efficient, the resulted intensities for DQ coherences are even weaker and may be too weak to observe. In fact, the direct *BB* DQ correlation intensity is already weak since the intermolecular CH-CH distance is about 3.6 Å [82] (Fig. 3a), not to mention the TQ correlations, *ABB*, and *BBC* (Fig. 3b). Therefore, the negligible *BB* DQ correlation in the projected 2D DQ/SQ spectrum can be ascribed to the weak intensity of TQ coherences involving two methine groups. As for TQ spectra, no additional peak appears in the projected TQ/SQ spectrum compared to the regular TQ/SQ spectrum on contrary to the DQ spectrum. This is because the TQ coherences are both excited from the same initial equilibrium state, i.e. the magnetization in equilibrium is along the +z direction before the TQ coherence excitation. Nevertheless, the signal intensities in the projected TQ/SQ spectrum are much weaker due to the polarization transfer via DQ coherences, leading to significant signal loss. Although the TQ/SQ spectrum provides unambiguous three-spin correlation information, all the correlation peaks are still overlapped with each other, rendering it difficult for clear TQ resonance assignments to probing three-spin proximity especially when

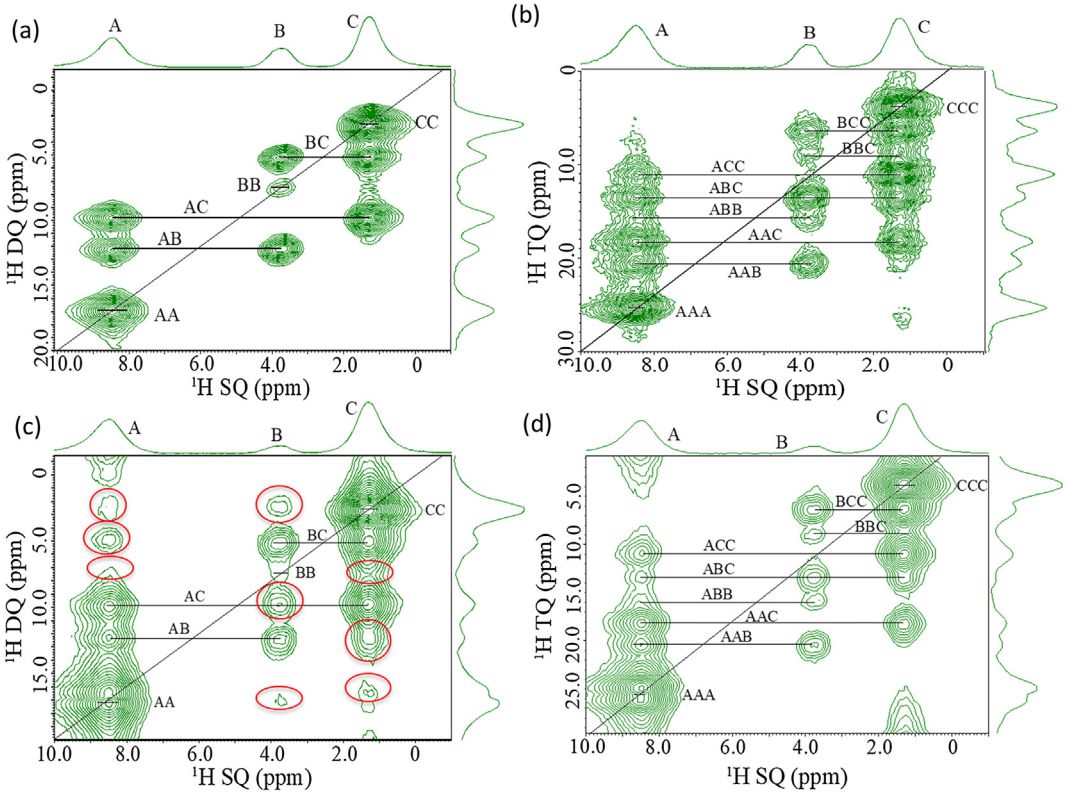

Fig. 3. Comparison of 2D DQ/SQ and TQ/SQ spectra obtained from the regular 2D experiment (a, b) and projections of the 3D TQ/DQ/SQ spectrum (c, d). (a) 2D DQ/SQ spectrum obtained from the 2D DQ/SQ experiment (pulse sequence shown in Fig. S2a); (b) 2D TQ/SQ spectrum obtained from the 2D TQ/SQ experiment (pulse sequence shown in Fig. S2b); (c) 2D DQ/SQ spectrum obtained from the projection of the 3D TQ/DQ/SQ spectrum, where the red circles indicate the additional correlation peaks between a spin pair and another spin, since the DQ coherences in the 3D experiment are converted from the TQ coherences; (d) 2D TQ/SQ spectrum obtained from the projection of the 3D TQ/DQ/SQ spectrum. For simplifying the representations, we used label *A*, *B*, *C* to denote the protons of —NH_3^+, —CH and —CH_3 groups, respectively. (For interpretation of the references to colour in this figure legend, the reader is referred to the web version of this article.)

more proton peaks are present in the case of MLF as will be shown below.

For further simplifying the extraction of spin proximity information, we can take the TQ/DQ slice at a specific isotropic SQ chemical shift where the DQ and TQ chemical shift are the sum of the isotropic chemical shifts of two and three protons, respectively. A schematic cartoon is shown in Fig. 4a in order to explain the procedures for resonance assignments. The below procedures can be taken to accurately assign the correlation peaks:

(1) Pick a peak, for example, the peak at a chemical shift of ω_A (spin *A*) on the 1D SQ spectrum;
(2) Resolve a DQ correlation peak (involving spin *A*) from the projected DQ/SQ spectrum. For example, spin *A* and *C* are correlated at a DQ chemical shift of $\omega_A + \omega_C$;
(3) Take a TQ/DQ slice at the SQ chemical shift of ω_A from the 3D TQ/DQ/SQ spectrum, and identify all the TQ correlation peaks at the DQ chemical shift of $\omega_A + \omega_C$. Plot the diagonal line where the DQ chemical shift is the same as the TQ chemical shift, i.e. diagonal line with a slope of 1;
(4) Overlay the 1D SQ spectrum on to the TQ/DQ slice along the TQ dimension at the DQ chemical shift of $\omega_A + \omega_C$. The chemical shift range of the 1D SQ spectrum has to be [0, δ_t-ω_A-ω_C], where δ_t is the upper bound chemical shift value along the TQ dimension of the shown TQ/DQ slice. In addition, the 0 ppm position of the 1D SQ spectrum has to be on the diagonal line of the sliced TQ/DQ spectrum. In this case, if the TQ/DQ contour peak is overlaid with a peak of the 1D SQ spectrum, it means that the spin, indicated by this overlaid SQ chemical shift, is the third spin involved in inducing TQ coherence together with spin *A* and *C*. For example, in the cartoon, it indicates that there are three different TQ chemical shift values induced by the spins *ACC*, *ABC*, and *AAC*, indicating three different spin clusters in close proximity.

Here, taking alanine for example, we can well resolve the DQ correlation between NH_3^+ group (denoted as spin *A*, Fig. 3) and —CH group (denoted as spin *B*, Fig. 3) from the regular DQ/SQ (Fig. 3a) or projected DQ/SQ (Fig. 3c) spectrum, where the DQ chemical shift between spin *A* and *B* is around 12.1 ppm. Then extract the TQ/DQ slice at the SQ chemical shift of *B* from the 3D spectrum and overlay the 1D spectrum of alanine onto the TQ/DQ slice along the TQ dimension at the DQ chemical shift of 12.1 ppm, as shown in Fig. 4b. Therefore, at the DQ chemical shift of 12.1 ppm, the three TQ/DQ correlation contour peaks in the TQ/DQ slice can be identified as results from the three-spin correlations of *AAB*, *ABB*, and *ABC*. It is worth noting that in Fig. 4b there is another correlation peak at the DQ chemical shift of 17.4 ppm. This DQ chemical shift does not involve spin *B*, and is decomposed to the correlation of *AA*. Thus, the three-spin correlation can be directly ascribed to *AAB*, since the TQ/DQ spectrum is sliced at the SQ chemical shift of spin *B*. These correlations appear on the line parallel to the diagonal line with the distance of isotropic chemical shift of spin *B* (dotted line in Fig. 4b). To a large degree, the TQ/DQ slice contains unambiguous correlation information since it is only related to the specific proton, and the assignment can be easily achieved as explained above. Herein, the 3D experiment not only provides general two- and three-spin proximity information, but also can offer the local proton proximity information and simplify the resonance assignment by taking the TQ/DQ slice at a specific SQ chemical shift.

3.3. 3D TQ/DQ/SQ Spectrum of MLF at 72 kHz MAS and 900 MHz Magnetic Field

To further demonstrate the feasibility of the 3D experiment presented in this study, we extended the demonstration of the 3D experiment on a tripeptide powder sample of MLF at 72 kHz MAS and 900 MHz magnetic field. The high-resolution proton spectrum of MLF along with the chemical structure and resonance assignments is shown in Fig. 5. For simplifying the representation, we use numbers (***1,2,3***...) to indicate the proton peaks below in the 1D and 2D spectra, and their corresponding assignments can be found in the inset table according to the work by Nishiyama with some minor corrections [83]. Peak ***2***, ***3*** and ***4*** are assigned to (M-COH, L-NH), (M-NH), and (F-NH, F-Hδ, -Hε, -Hζ), respectively. The high resolution proton spectra of MLF under ultrafast MAS up to 70 kHz under the 600 MHz magnetic field were previously reported [83]. Here, higher resolution is achieved thanks to the 900 MHz magnetic field and a spinning rate of 72 kHz, in particular on the aliphatic region between 0 and 5 ppm, demonstrating the benefits of ultrahigh magnetic field for achieving high spectral resolution in the proton-based NMR studies.

The 2D DQ/SQ, TQ/SQ and TQ/DQ projections from the 3D spectra of MLF are shown in Fig. 6, while the regular 2D DQ/SQ and TQ/SQ spectra are shown in Fig. S6. Compared to the regular 2D DQ/SQ and TQ/SQ spectra, the projected 2D DQ/SQ and TQ/SQ

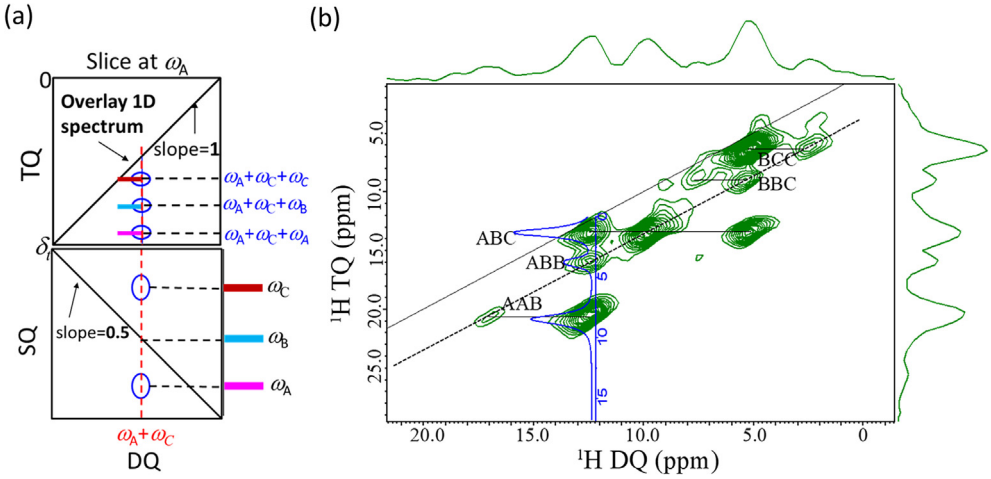

Fig. 4. (a) Schematic illustration of identifying the three spins involved in TQ coherences. (b) The TQ/DQ slice taken at the isotropic SQ chemical shift of —CH group of alanine. For simplifying the representation, we used label *A*, *B*, and *C* to denote the protons of —NH_3^+, —CH and —CH_3 groups, respectively. The solid line indicates the diagonal line with a slope of 1, while the dot line is in parallel with the solid line at a distance of the isotropic chemical shift of spin *B*.

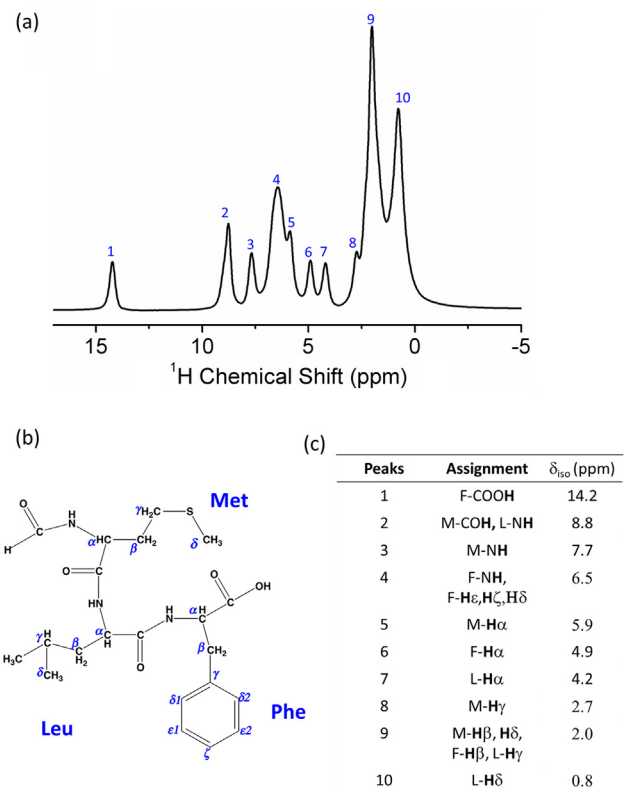

Peaks	Assignment	δ_{iso} (ppm)
1	F-COOH	14.2
2	M-COH, L-NH	8.8
3	M-NH	7.7
4	F-NH, F-Hε,Hζ,Hδ	6.5
5	M-Hα	5.9
6	F-Hα	4.9
7	L-Hα	4.2
8	M-Hγ	2.7
9	M-Hβ, Hδ, F-Hβ, L-Hγ	2.0
10	L-Hδ	0.8

Fig. 5. (a) ^{1}H spectrum of MLF with numbers to indicate different peaks; (b) Molecular structure of N-formyl-*L*-methionyl-*L*-leucyl-*L*-phenylalanine (MLF) with the labels for the hydrogen atoms. (c) Chemical shifts and resonance assignment for each peak in the proton spectrum. In the table, the letter *M, L, F* indicates the amino acid of *L*-methionyl, and *L*-leucyl, *L*-phenylalanine in MLF, respectively.

spectra show much less correlation peaks, which can be ascribed to the fact that some signals are too weak to observe due to the severe signal loss for the $I_{nz} \rightarrow$ TQ $\rightarrow$ DQ $\rightarrow$ SQ coherence transition processes and/or in lesser extent the finite time evolution (one rotor period) before the t_2 evolution. Notably, we observe several additional DQ/SQ correlation peaks (indicated by the dashed red circles) in the projected 2D DQ/SQ spectrum (Fig. 6a), which are not observed in the regular 2D DQ/SQ spectrum (Fig. S6a). These correlations peaks are resulted from the three-spin DQ correlations as discussed above in the case of alanine. Three-spin correlations can also be straightforwardly obtained from the TQ/SQ correlation spectrum. However, as shown in both Figs. 6b and S6b, there are too many overlapped peaks since the TQ chemical shift is the sum of the SQ chemical shifts of three spins, making the results hard to interpret. As a result, the projected TQ/DQ spectrum also shows severely overlapped peaks (Fig. 6c) and renders the data interpretation more difficult. However, such severe peak overlapping can be greatly alleviated by taking the TQ/DQ slices at specific SQ chemical shifts as shown in Fig. 7.

Fig. 7 shows the TQ/DQ spectra sliced at the isotropic SQ chemical shift of 14.2 ppm (F-COOH, spin ***1***), 8.8 ppm (M-COH and L-NH, spin ***2***) and 7.7 ppm (M-NH, spin ***3***), which only contain local proton proximity information related to the specific proton spins. As seen in Fig. 7a–7c, correlation involving both spin ***1*** and ***2*** is clearly observed, and the strong correlation involving spin ***1***, ***2***, ***3*** is observed in all three slices taken at the SQ chemical shift of spin ***1***, ***2***, and ***3*** as expected. This clearly shows the formation of (***1***, ***2***, ***3***) three-spin cluster. In fact, the intermolecular distances for (***1***: F-COOH, ***2***: M-COH) and (***1***: F-COOH, ***3***: M-NH) are about 2.7 Å and 1.8 Å, respectively, and the intramolecular distance for (***2***:

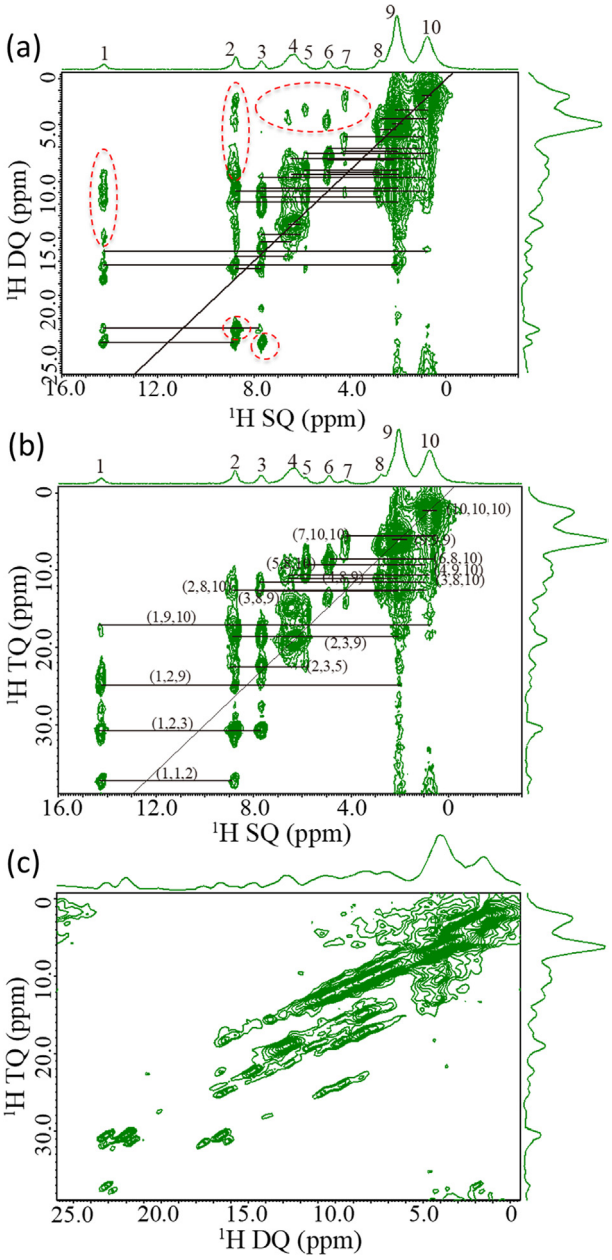

Fig. 6. 2D (a) DQ/SQ, (b) TQ/SQ and (c) TQ/DQ projections extracted from the 3D TQ/DQ/SQ spectrum of MLF. Some additional correlation peaks, corresponding to the correlation between a spin pair and another spin, are also observed as indicated by the dash red circles. (For interpretation of the references to colour in this figure legend, the reader is referred to the web version of this article.)

M-COH, ***3***: M-NH) is around 1.9 Å [84]. On the other hand, the intermolecular distances for (***1***: F-COOH, ***2***: L-NH), (***1***: F-COOH, ***3***: M-NH), and (***2***: L-NH, ***3***: M-NH) are 4.0 Å, 1.8 Å, and 3.1 Å, respectively [84]. Those distances are in a good range for inducing DQ coherences. Therefore, the three-spin (***1***,***2***,***3***) TQ correlation is the contribution of two clusters (***1***: F-COOH, ***2***: M-COH, ***3***: M-NH) and (***1***: F-COOH, ***2***: L-NH, ***3***: M-NH). The advantages of 3D TQ/DQ/SQ experiment over 2D TQ/SQ and DQ/SQ experiments are highlighted especially when analyzing the crowded area. For example, although the DQ correlations between spin ***2*** and ***3*** are observed in the DQ/SQ correlation experiment, it is ambiguous to read three-spin correlations with spin ***2*** and ***3*** in the TQ/SQ correlation experiment due to severe spectral overlaps. However, these peaks can easily be assigned through the TQ/DQ slices at the SQ

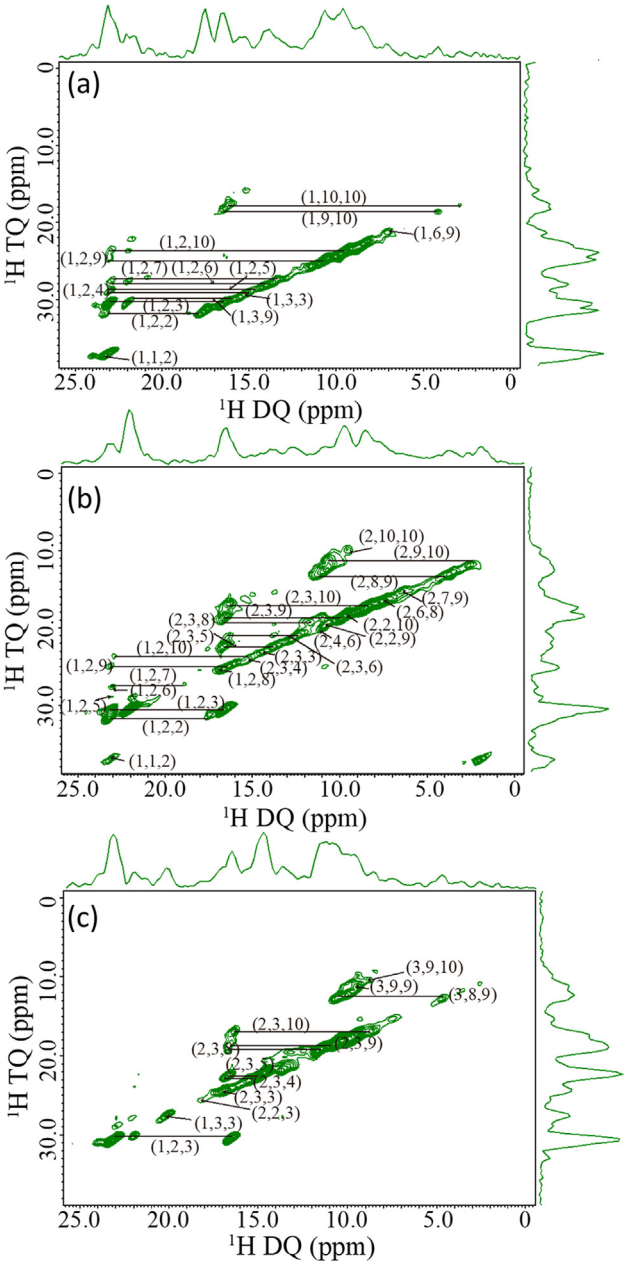

Fig. 7. 2D TQ/DQ spectra sliced at the SQ chemical shift of (a) 14.2 ppm (F-COOH, peak ***1***), (b) 8.8 ppm (M-COH and L-NH, peak ***2***) and (c) 7.7 ppm (M-NH, peak ***3***) of the 3D TQ/DQ/SQ spectrum.

chemical shift of spin ***2,*** 8.8 ppm (Fig. 7b). As schematically shown in the cartoon in Fig. 4, overlaying 1D spectrum into the 2D TQ/DQ slice at the DQ chemical shift of 16.5 ppm (i.e. spins (***2***,***3***)) in Fig. 7b provides clear TQ correlations of (***2***,***3***,***1***), (***2***,***3***,***2***), (***2***,***3***,***5***), (***2***,***3***,***6***), (***2***,***3***,***8***), (***2***,***3***,***9***) and (***2***,***3***,***10***) (see Fig. S7). It is worth noting that spin ***9*** consists of 4 protons and not all of them create the three-spin correlation with DQ correlations of (***2***,***3***). These correlations are not readily available in the 2D TQ/SQ correlation spectrum. It should be emphasized that the excitation of TQ coherences only requires two spin pairs sharing one common spin between these pairs. It means that the TQ coherence (*A, B, C*) can still be observed even in the small or absence of dipolar coupling of *AC*, if both spin pairs *AB* and *BC* can induce the DQ coherences. As a result, the (***1***, ***2***, ***2***) TQ coherence appears at a DQ frequency of 23.0 ppm from two (***1,2***) pairs, leading to two evident TQ/DQ contour peaks in the sliced TQ/DQ spectrum (Fig. 7a and 7b) despite the negligible (***2***,***2***) DQ correlation appearing in the DQ/SQ spectrum (see Fig. 6a). The negligible (***2***,***2***) DQ correlation is ascribed to the long intermolecular distance of ~4.8 Å between 2:M-COH and 2: L-NH [84]. On the other hand, shorter distances of 2.7 Å and 3.9 Å can be found both for (1: F-COOH, 2:M-COH) and (1: F-COOH, 2:L-NH), respectively, leading to strong (***1***, ***2***) DQ correlations. It is worth noting that we also observe a three-spin correlation (***1,1,2***) in the 2D TQ/SQ spectra (Fig. 6b and S6b) and the TQ/DQ slices at a SQ chemical shift of 14.2 ppm (Fig. 7a) and 8.8 ppm (Fig. 7b), although no (***1***,***1***) DQ correlation is observed in the 2D DQ/SQ spectrum (Fig. S6a). The (***1***,***1***,***2***) correlation does not match to the reported crystalline structure [84], since there is no (***1***,***1***,***2***) spin cluster in the proximity shorter than 5 Å. We believe one possible reason is because our sample has a different crystalline form from the reported crystalline structure. Interestingly, from Fig. 7a and 7b, we see many TQ/DQ correlation peaks at the DQ chemical shift of around 22.9 ppm (i.e. DQ correlation (***1,2***)). This means that among the three-spin clusters, the polarization transfer between spin ***1*** and ***2*** dominates the other transfer processes. Following the procedures explained above, those TQ/DQ correlation peaks can be unambiguously assigned.

4. Conclusion

In summary, we have proposed a single-channel proton 3D TQ/DQ/SQ chemical shift correlation experiment to probe two-spin and three-spin proximity under ultrafast MAS beyond 70 kHz, which has been well demonstrated to significantly enhance the spectral resolution. In addition to the two-spin proximity and more accurate three-spin proximity information offered by the projected DQ/SQ and TQ/SQ spectrum, respectively, the TQ/DQ slices only contain the local proton proximity information related to the specific proton spins indicated by the isotropic SQ chemical shifts. Therefore, it can aid in assigning the overlapped peaks along the TQ or DQ dimensions and thus simplify the data interpretation of DQ and TQ spectra. Overall, we believe that the elegant 3D ^{1}H TQ/DQ/SQ experiment under ultrafast MAS will be greatly beneficial for probing the proximity among different proton spins and thus enable high-throughput investigations of structures and dynamics of various materials and proteins. Such structural characterizations can further benefit from the use of faster MAS (such as 140 kHz), higher external magnetic field (such as 1.5 GHz) as well as partial deuteration of samples.

Declaration of Competing Interest

There are no conflicts to declare.

Acknowledgements

We would like to acknowledge Prof. Vipin Agarwal of TIFR Hyderabad for useful discussion. R. Zhang acknowledges the financial support of National Natural Science Foundation of China (No. 21704046), Guangdong Innovative and Entrepreneurial Research Team Program (No. 2016ZT06C322), and the startup funds from South China University of Technology.

Appendix A. Supplementary data

Supplementary data to this article can be found online at https://doi.org/10.1016/j.jmr.2019.05.006.

References

[1] K. Schmidt-Rohr, H.W. Spiess, Multidimensional solid-state NMR and polymers, Academic Press, 1994.

[2] F. Separovic, A. Natio (Eds.), Advances in Biological Solid-State NMR: Proteins and Membrane-Active Peptides, Royal Society of Chemistry, Cambridge, 2014.
[3] P. Hodgkinson (Ed.), Modern Methods in Solid-State NMR: A Practitioner's Guide, Royal Society of Chemistry, Cambridge, 2018.
[4] M.R. Hansen, R. Graf, H.W. Spiess, Interplay of structure and dynamics in functional macromolecular and supramolecular systems as revealed by magnetic resonance spectroscopy, Chem. Rev. 116 (2015) 272–1308.
[5] J.R. Lewandowski, M.E. Halse, M. Blackledge, L. Emsley, Direct observation of hierarchical protein dynamics, Science 348 (2015) 578–581.
[6] Y. Xiao, B. Ma, D. McElheny, S. Parthasarathy, F. Long, M. Hoshi, R. Nussinov, Y. Ishii, Aβ (1–42) fibril structure illuminates self-recognition and replication of amyloid in Alzheimer's disease, Nat. Struct. Mol. Biol. 22 (2015) 499.
[7] J. Stanek, L.B. Andreas, K. Jaudzems, D. Cala, D. Lalli, A. Bertarello, T. Schubeis, I. Akopjana, S. Kotelovica, K. Tars, A. Pica, S. Leone, D. Picone, Z.-Q. Xu, N.E. Dixon, D. Martinez, M. Berbon, N. El Mammeri, A. Noubhani, S. Saupe, B. Habenstein, A. Loquet, G. Pintacuda, NMR spectroscopic assignment of backbone and side-chain protons in fully protonated proteins: microcrystals, sedimented assemblies, and amyloid fibrils, Angew. Chem. Int. Ed. 55 (2016) 15504–15509.
[8] W. Qiang, W.-M. Yau, J.-X. Lu, J. Collinge, R. Tycko, Structural variation in amyloid-β fibrils from Alzheimer's disease clinical subtypes, Nature 541 (2017) 217.
[9] J.T. Damron, J. Ma, R. Kurz, K. Saalwächter, A.J. Matzger, A. Ramamoorthy, The influence of chemical modification on linker rotational dynamics in metal organic frameworks, Angew. Chem. 130 (2018) 8814–8817.
[10] G. Cho, Y. Wu, J.L. Ackerman, Detection of hydroxyl ions in bone mineral by solid-state NMR spectroscopy, Science 300 (2003) 1123–1127.
[11] P. Zhu, J. Xu, N. Sahar, M.D. Morris, D.H. Kohn, A. Ramamoorthy, Time-resolved dehydration-induced structural changes in an intact bovine cortical bone revealed by solid-state NMR spectroscopy, J. Am. Chem. Soc. 131 (2009) 17064–17065.
[12] V.S. Mandala, J.K. Williams, M. Hong, Structure and dynamics of membrane proteins from solid-state NMR, Annu. Rev. Biophys. 47 (2018) 201–222.
[13] S. Wang, V. Ladizhansky, Recent advances in magic angle spinning solid state NMR of membrane proteins, Prog. Nucl. Magn. Reson. Spectrosc. 82 (2014) 1–26.
[14] B.H. Meier, R. Riek, A. Böckmann, Emerging structural understanding of amyloid fibrils by solid-state NMR, Trends Biochem. Sci. 42 (2017) 777–787.
[15] A. Goldbourt, Biomolecular magic-angle spinning solid-state NMR: recent methods and applications, Curr. Opin. Biotechnol. 24 (2013) 705–715.
[16] P.C.A. van der Wel, Insights into protein misfolding and aggregation enabled by solid-state NMR spectroscopy, Solid State Nucl. Magn. Reason. 88 (2017) 1–14.
[17] R. Zhang, K.H. Mroue, A. Ramamoorthy, Proton-based ultrafast magic angle spinning solid-state NMR spectroscopy, Acc. Chem. Res. 50 (2017) 1105–1113.
[18] Y. Nishiyama, Fast magic-angle sample spinning solid-state NMR at 60–100 kHz for natural abundance samples, Solid State Nucl. Magn. Reson. 78 (2016) 24–36.
[19] K.R. Mote, V. Agarwal, P.K. Madhu, Five decades of homonuclear dipolar decoupling in solid-state NMR: status and outlook, Prog. Nucl. Magn. Reson. Spectrosc. 97 (2016) 1–39.
[20] Y.-L. Lin, Y.-S. Cheng, C.-I. Ho, Z.-H. Guo, S.-J. Huang, M.-L. Org, A. Oss, A. Samoson, J.C.C. Chan, Preparation of fibril nuclei of beta-amyloid peptides in reverse micelles, Chem. Commun. 54 (2018) 10459–10462.
[21] S. Penzel, A. Oss, M.-L. Org, A. Samoson, A. Böckmann, M. Ernst, B.H. Meier, Spinning faster: protein NMR at MAS frequencies up to 126 kHz, J. Biomol. NMR 73 (2019) 19–29.
[22] A. Böckmann, M. Ernst, B.H. Meier, Spinning proteins, the faster, the better?, J Magn. Reson. 253 (2015) 71–79.
[23] U. Sternberg, R. Witter, I. Kuprov, J.M. Lamley, A. Oss, J.R. Lewandowski, A. Samoson, 1H line width dependence on MAS speed in solid state NMR – Comparison of experiment and simulation, J. Magn. Reson. 291 (2018) 32–39.
[24] T. Schubeis, T. Le Marchand, L.B. Andreas, G. Pintacuda, 1H magic-angle spinning NMR evolves as a powerful new tool for membrane proteins, J. Magn. Reson. 287 (2018) 140–152.
[25] Y. Ishii, A. Wickramasinghe, I. Matsuda, Y. Endo, Y. Ishii, Y. Nishiyama, T. Nemoto, T. Kamihara, Progress in proton-detected solid-state NMR (SSNMR): Super-fast 2D SSNMR collection for nano-mole-scale proteins, J. Magn. Reson. 286 (2018) 99–109.
[26] Y. Nishiyama, Solid-state NMR under ultrafast MAS rate of 40–120 kHz, in: Experimental Approaches of NMR Spectroscopy: Methodology and Application to Life Science and Materials Science, The Nuclear Magnetic Resonance Society of Japan, Springer, 2018, pp. 171–195.
[27] S.K. Vasa, P. Rovó, R. Linser, Protons as versatile reporters in solid-state NMR spectroscopy, Acc. Chem. Res. 51 (2018) 1386–1395.
[28] S. Asami, B. Reif, Proton-detected solid-state NMR spectroscopy at aliphatic sites: application to crystalline systems, Acc. Chem. Res. 46 (2013) 2089–2097.
[29] D.H. Zhou, G. Shah, M. Cormos, C. Mullen, D. Sandoz, C.M. Rienstra, Proton-detected solid-state NMR spectroscopy of fully protonated proteins at 40 kHz magic-angle spinning, J. Am. Chem. Soc. 129 (2007) 11791–11801.
[30] Y. Ishii, J.P. Yesinowski, R. Tycko, Sensitivity enhancement in solid-state 13C NMR of synthetic polymers and biopolymers by 1H NMR detection with high-speed magic angle spinning, J. Am. Chem. Soc. 123 (2001) 2921–2922.
[31] A. Samoson, T. Tuherm, Z. Gan, High-field high-speed MAS resolution enhancement in 1H NMR spectroscopy of solids, Solid State Nucl. Magn. Reson. 20 (2001) 130–136.
[32] V.E. Zorin, S.P. Brown, P. Hodgkinson, Origins of linewidth in [sup 1]H magic-angle spinning NMR, J. Chem. Phys. 125 (2006) 144508.
[33] M. Huber, S. Hiller, P. Schanda, M. Ernst, A. Böckmann, R. Verel, B.H. Meier, A proton-detected 4D solid-state NMR experiment for protein structure determination, ChemPhysChem 12 (2011) 915–918.
[34] R. Linser, M. Dasari, M. Hiller, V. Higman, U. Fink, J.-M. Lopez del Amo, S. Markovic, L. Handel, B. Kessler, P. Schmieder, D. Oesterhelt, H. Oschkinat, B. Reif, Proton-detected solid-state NMR spectroscopy of fibrillar and membrane proteins, Angew. Chem. Int. Ed. 50 (2011) 4508–4512.
[35] M.E. Ward, L. Shi, E. Lake, S. Krishnamurthy, H. Hutchins, L.S. Brown, V. Ladizhansky, Proton-detected solid-state NMR reveals intramembrane polar networks in a seven-helical transmembrane protein proteorhodopsin, J. Am. Chem. Soc. 133 (2011) 17434–17443.
[36] V. Agarwal, S. Penzel, K. Szekely, R. Cadalbert, E. Testori, A. Oss, J. Past, A. Samoson, M. Ernst, A. Böckmann, B.H. Meier, De Novo 3D structure determination from sub-milligram protein samples by solid-state 100 kHz MAS NMR spectroscopy, Angew. Chem. Int. Ed. 53 (2014) 1–5.
[37] E. Barbet-Massin, A.J. Pell, J.S. Retel, L.B. Andreas, K. Jaudzems, W.T. Franks, A.J. Nieuwkoop, M. Hiller, V. Higman, P. Guerry, A. Bertarello, M.J. Knight, M. Felletti, T. Le Marchand, S. Kotelovica, I. Akopjana, K. Tars, M. Stoppini, V. Bellotti, M. Bolognesi, S. Ricagno, J.J. Chou, R.G. Griffin, H. Oschkinat, A. Lesage, L. Emsley, T. Herrmann, G. Pintacuda, Rapid proton-detected NMR assignment for proteins with fast magic angle spinning, J. Am. Chem. Soc. 136 (2014) 12489–12497.
[38] G.P. Holland, B.R. Cherry, J.E. Jenkins, J.L. Yarger, Proton-detected heteronuclear single quantum correlation NMR spectroscopy in rigid solids with ultra-fast MAS, J. Magn. Reson. 202 (2010) 64–71.
[39] Y. Nishiyama, Y. Endo, T. Nemoto, H. Utsumi, K. Yamauchi, K. Hioka, T. Asakura, Very fast magic angle spinning 1H–14N 2D solid-state NMR: Sub-micro-liter sample data collection in a few minutes, J. Magn. Reson. 208 (2011) 44–48.
[40] B. Reif, Ultra-high resolution in MAS solid-state NMR of perdeuterated proteins: implications for structure and dynamics, J. Magn. Reson. 216 (2012) 1–12.
[41] L.B. Andreas, T. Le Marchand, K. Jaudzems, G. Pintacuda, High-resolution proton-detected NMR of proteins at very fast MAS, J. Magn. Reson. 253 (2015) 36–49.
[42] K.H. Mroue, Y. Nishiyama, M. Kumar Pandey, B. Gong, E. McNerny, D.H. Kohn, M.D. Morris, A. Ramamoorthy, Proton-detected solid-state NMR spectroscopy of bone with ultrafast magic angle spinning, Sci. Rep. 5 (2015) 11991.
[43] Y. Nishiyama, M. Malon, M.J. Potrzebowski, P. Paluch, J.P. Amoureux, Accurate NMR determination of C–H or N–H distances for unlabeled molecules, Solid State Nucl. Magn. Reson. 73 (2016) 15–21.
[44] D. Cala-De Paepe, J. Stanek, K. Jaudzems, K. Tars, L.B. Andreas, G. Pintacuda, Is protein deuteration beneficial for proton detected solid-state NMR at and above 100 kHz magic-angle spinning?, Solid State Nucl Magn. Reson. 87 (2017) 126–136.
[45] J. Struppe, C.M. Quinn, M. Lu, M. Wang, G. Hou, X. Lu, J. Kraus, L.B. Andreas, J. Stanek, D. Lalli, A. Lesage, G. Pintacuda, W. Maas, A.M. Gronenborn, T. Polenova, Expanding the horizons for structural analysis of fully protonated protein assemblies by NMR spectroscopy at MAS frequencies above 100 kHz, Solid State Nucl. Magn. Reson. 87 (2017) 117–125.
[46] M. Makrinich, A. Goldbourt, 1H-Detected quadrupolar spin–lattice relaxation measurements under magic-angle spinning solid-state NMR, Chem. Commun. 55 (2019) 5643–5646.
[47] M.G. Jain, K.R. Mote, P.K. Madhu, NMR crystallography at fast magic-angle spinning frequencies: application of novel recoupling methods, Crystals 9 (2019) 231.
[48] X. Lu, D. Skomski, K.C. Thompson, M.J. McNevin, W. Xu, Y. Su, Three-dimensional NMR spectroscopy of fluorinated pharmaceutical solids under ultrafast magic angle spinning, Anal. Chem. 91 (2019) 6217–6224.
[49] Y. Nishiyama, T. Kobayashi, M. Malon, D. Singappuli-Arachchige, I.I. Slowing, M. Pruski, Studies of minute quantities of natural abundance molecules using 2D heteronuclear correlation spectroscopy under 100 kHz MAS, Solid State Nucl. Magn. Reson. 66–67 (2015) 56–61.
[50] A.K. Chattah, R. Zhang, K.H. Mroue, L.Y. Pfund, M.R. Longhi, A. Ramamoorthy, C. Garnero, Investigating albendazole desmotropes by solid-state NMR spectroscopy, Mol. Phamaceutics 12 (2015) 731–741.
[51] R. Zhang, A. Ramamoorthy, Constant-time 2D and 3D through-bond correlation NMR spectroscopy of solids under 60 kHz MAS, J. Chem. Phys. 144 (2016) 034202.
[52] D.H. Zhou, C.M. Rienstra, Rapid analysis of organic compounds by proton-detected heteronuclear correlation NMR spectroscopy with 40 kHz magic-angle spinning, Angew. Chem. 120 (2008) 7438–7441.
[53] G.N.M. Reddy, A. Marsh, J.T. Davis, S. Masiero, S.P. Brown, Interplay of noncovalent interactions in ribbon-like guanosine self-assembly: an NMR crystallography study, Cryst. Growth Des. 5945–5954 (2015).
[54] G.N.M. Reddy, M. Malon, A. Marsh, Y. Nishiyama, S.P. Brown, Fast magic-angle spinning three-dimensional NMR experiment for simultaneously probing H–H and N–H proximities in solids, Anal. Chem. 88 (2016) 11412–11419.
[55] A.S. Tatton, H. Blade, S.P. Brown, P. Hodgkinson, L.P. Hughes, S.O.N. Lill, J.R. Yates, Improving confidence in crystal structure solutions using NMR crystallography: the case of β-piroxicam, Cryst. Growth Des. 18 (2018) 3339–3351.
[56] V. Chevelkov, K. Rehbein, A. Diehl, B. Reif, Ultrahigh resolution in proton solid-state NMR spectroscopy at high levels of deuteration, Angew. Chem. Int. Ed. 45 (2006) 3878–3881.

[57] V. Chevelkov, A. Diehl, B. Reif, Measurement of N15–T1 relaxation rates in a perdeuterated protein by magic angle spinning solid-state nuclear magnetic resonance spectroscopy, J. Chem. Phys. 128 (2008) 052316.
[58] Ü. Akbey, S. Lange, W. Trent Franks, R. Linser, K. Rehbein, A. Diehl, B.-J. van Rossum, B. Reif, H. Oschkinat, Optimum levels of exchangeable protons in perdeuterated proteins for proton detection in MAS solid-state NMR spectroscopy, J. Biomol. NMR 46 (2010) 67–73.
[59] Y. Nishiyama, M. Malon, Y. Ishii, A. Ramamoorthy, 3D 15N/15N/1H chemical shift correlation experiment utilizing an RFDR-based 1H/1H mixing period at 100kHz MAS, J. Magn. Reson. 244 (2014) 1–5.
[60] D.H. Brouwer, J.A. Ripmeester, Symmetry-based recoupling of proton chemical shift anisotropies in ultrahigh-field solid-state NMR, J. Magn. Reson. 185 (2007) 173–178.
[61] H.K. Miah, D.A. Bennett, D. Iuga, J.J. Titman, Measuring proton shift tensors with ultrafast MAS NMR, J. Magn. Reson. 235 (2013) 1–5.
[62] M.K. Pandey, M. Malon, A. Ramamoorthy, Y. Nishiyama, Composite-180° pulse-based symmetry sequences to recouple proton chemical shift anisotropy tensors under ultrafast MAS solid-state NMR spectroscopy, J. Magn. Reson. 250 (2015) 45–64.
[63] R. Zhang, K.H. Mroue, A. Ramamoorthy, Proton chemical shift tensors determined by 3D ultrafast MAS double-quantum NMR spectroscopy, J. Chem. Phys. 143 (2015) 144201.
[64] L. Liang, G. Hou, X. Bao, Measurement of proton chemical shift anisotropy in solid-state NMR spectroscopy, Solid State Nucl. Magn. Reson. 93 (2018) 16–28.
[65] G. Hou, R. Gupta, T. Polenova, A.J. Vega, A magic-angle-spinning NMR spectroscopy method for the site-specific measurement of proton chemical-shift anisotropy in biological and organic solids, Isr. J. Chem. 54 (2014) 171–183.
[66] G. Hou, S. Paramasivam, S. Yan, T. Polenova, A.J. Vega, Multidimensional magic angle spinning NMR spectroscopy for site-resolved measurement of proton chemical shift anisotropy in biological solids, J. Am. Chem. Soc. 135 (2013) 1358–1368.
[67] R. Zhang, K.H. Mroue, P. Sun, A. Ramamoorthy, High-resolution proton NMR spectroscopy of polymers and biological solids, in: G.A. Webb (Ed.), Modern Magnetic Resonance, Springer International Publishing, Cham, 2018.
[68] S.P. Brown, Probing proton–proton proximities in the solid state, Prog. Nucl. Magn. Reason. Spectrosc. 50 (2007) 199–251.
[69] Y. Nishiyama, R. Zhang, A. Ramamoorthy, Finite-pulse radio frequency driven recoupling with phase cycling for 2D 1H/1H correlation at ultrafast MAS frequencies, J. Magn. Reson. 243 (2014) 25–32.
[70] R. Zhang, Y. Nishiyama, P. Sun, A. Ramamoorthy, Phase cycling schemes for finite-pulse-RFDR MAS solid state NMR experiments, J. Magn. Reason. 252 (2015) 55–66.
[71] I. Schnell, A. Lupulescu, S. Hafner, D.E. Demco, H.W. Spiess, Resolution enhancement in multiple-quantum MAS NMR spectroscopy, J. Magn. Reson. 133 (1998) 61–69.
[72] R. Zhang, M.K. Pandey, Y. Nishiyama, A. Ramamoorthy, A novel high-resolution and sensitivity-enhanced three-dimensional solid-state NMR experiment under ultrafast magic angle spinning conditions, Sci. Rep. 5 (2015) 11810.
[73] R. Zhang, N.T. Duong, Y. Nishiyama, A. Ramamoorthy, 3D double-quantum/double-quantum exchange spectroscopy of protons under 100 kHz magic angle spinning, J. Phys. Chem. B 121 (2017) 5944–5952.
[74] T. Kobayashi, D. Singappuli-Arachchige, I.I. Slowing, M. Pruski, Spatial distribution of organic functional groups supported on mesoporous silica nanoparticles (2): a study by 1H triple-quantum fast-MAS solid-state NMR, Phys. Chem. Chem. Phys. 20 (2018) 22203–22209.
[75] U. Friedrich, I. Schnell, D.E. Demco, H.W. Spiess, Triple-quantum NMR spectroscopy in dipolar solids, Chem. Phys. Lett. 285 (1998) 49–58.
[76] I. Schnell, H.W. Spiess, High-resolution 1H NMR spectroscopy in the solid state: very fast sample rotation and multiple-quantum coherences, J. Magn. Reson. 151 (2001) 153–227.
[77] K. Saalwächter, F. Lange, K. Matyjaszewski, C.-F. Huang, R. Graf, BaBa-xy16: Robust and broadband homonuclear DQ recoupling for applications in rigid and soft solids up to the highest MAS frequencies, J. Magn. Reson. 212 (2011) 204–215.
[78] D. Marion, M. Ikura, R. Tschudin, A. Bax, Rapid recording of 2D NMR spectra without phase cycling. Application to the study of hydrogen exchange in proteins, J. Magn. Reson. 85 (1989) 393–399.
[79] S.P. Brown, A. Lesage, B. Elena, L. Emsley, Probing proton−proton proximities in the solid state: high-resolution two-dimensional 1H−H double-quantum CRAMPS NMR spectroscopy, J. Am. Chem. Soc. 126 (2004) 13230–13231.
[80] M. Feike, D.E. Demco, R. Graf, J. Gottwald, S. Hafner, H.W. Spiess, Broadband multiple-quantum NMR spectroscopy, J. Magn. Reson., Ser A 122 (1996) 214–221.
[81] B. Hu, Q. Wang, O. Lafon, J. Trébosc, F. Deng, J.P. Amoureux, Robust and efficient spin-locked symmetry-based double-quantum homonuclear dipolar recoupling for probing 1H–1H proximity in the solid-state, J. Magn. Reson. 198 (2009) 41–48.
[82] M.S. Lehmann, T.F. Koetzle, W.C. Hamilton, Precision neutron diffraction structure determination of protein and nucleic acid components. I. Crystal and molecular structure of the amino acid L-alanine, J. Am. Chem. Soc. 94 (1972) 2657–2660.
[83] H. Colaux, Y. Nishiyama, Resolution enhancement in proton double quantum magic-angle spinning spectra by constant-time acquisition, Solid State Nucl. Magn. Reson. 87 (2017) 104–110.
[84] A. Morffew, I. Tickle, Formyl-methionine-leucine-phenylalanine-OH, Cryst. Struct. Commun 10 (1981) 781–788.